

Submitted to AJ; draft May 25, 2010

2MASS J20261584–2943124: An Unresolved L0.5 + T6 Spectral Binary¹

Christopher R. Gelino

*Infrared Processing and Analysis Center, MC 100-22, California Institute of Technology,
Pasadena, CA 91125, USA*

and

Adam J. Burgasser^{2,3}

*Center for Astrophysics and Space Science, University of California San Diego, La Jolla,
CA 92093, USA*

ABSTRACT

We identify the L dwarf 2MASS J20261584–2943124 as an unresolved spectral binary, based on low-resolution, near-infrared spectroscopy from IRTF/Spex. The data reveal a peculiar absorption feature at $1.6\ \mu\text{m}$, previously noted in the spectra of other very low-mass spectral binaries, which likely arises from overlapping FeH and CH₄ absorption bands in the blended light of an L dwarf/T dwarf pair. Spectral template matching analysis indicates component types of L0.5 and T6, with relative brightness $\Delta H = 4.2 \pm 0.6$. Laser guide star adaptive optics imaging observations with Keck/NIRC2 fail to resolve the source, indicating a maximum separation at the observing epoch of $0''.25$, or a projected separation

¹Some of the data presented herein were obtained at the W.M. Keck Observatory, which is operated as a scientific partnership among the California Institute of Technology, the University of California, and the National Aeronautics and Space Administration. The Observatory was made possible by the generous financial support of the W.M. Keck Foundation.

²Also Massachusetts Institute of Technology, Kavli Institute for Astrophysics and Space Research, Building 37, Room 664B, 77 Massachusetts Avenue, Cambridge, MA 02139, USA.

³Visiting Astronomer at the Infrared Telescope Facility, which is operated by the University of Hawai'i under Cooperative Agreement NCC 5-538 with the National Aeronautics and Space Administration, Office of Space Science, Planetary Astronomy Program.

of 9 AU assuming a distance of 36 ± 5 pc. With an age that is likely to be relatively older ($\gtrsim 5$ Gyr) based on the system’s large V_{tan} and mass ratio arguments, the relative motion of the potentially “massive” ($0.06\text{--}0.08 M_{\odot}$) components of 2MASS J2026–2943 may be detectable through radial velocity variations, like its earlier-type counterpart 2MASS J03202839–0446358 (M8+T5), providing dynamical mass measurements that span the hydrogen burning limit.

Subject headings: stars: binaries: general — stars: fundamental parameters — stars: individual (2MASS J20261584–2943124) — stars: low mass, brown dwarfs

1. Introduction

Multiple systems are of fundamental importance in stellar astrophysics and are particularly crucial for studies of very low mass stars (VLM; $M < 0.1 M_{\odot}$) and brown dwarfs, the M, L, and T dwarfs (see Kirkpatrick 2005 and references therein). The frequency and characteristics of VLM multiples provide empirical constraints for currently debated formation mechanisms (e.g., Burgasser et al. 2007b; Luhman et al. 2007a), and are the dominant outlet for direct mass and radius measurements (e.g., Lane et al. 2001; Zapatero Osorio et al. 2004; Stassun et al. 2006; Liu et al. 2008; Dupuy et al. 2009). Resolved VLM multiples provide useful laboratories for studying atmospheric properties independent of age and composition effects (e.g., Liu & Leggett 2005; Mohanty et al. 2007; Burgasser et al. 2010), and yield unique insights into evolutionary processes such as the poorly-understood L dwarf/T dwarf transition (e.g., Dahn et al. 2002; Liu et al. 2006; Burgasser 2007a; Looper et al. 2008a).

Current VLM multiplicity studies are dominated by resolved imaging programs, which have uncovered ~ 100 systems to date¹. These systems have constrained the frequency ($\sim 15\text{--}35\%$), and separation and mass ratio distributions of VLM multiples. Yet resolved imaging studies are insensitive to very closely-separated ($\rho < 1$ AU) and/or distant multiples, as well as multiples observed in unfortunate geometries (e.g., Martín et al. 1999; Liu & Leggett 2005; Gelino et al. 2006). The closely-separated systems are particularly valuable, as they are the ones most likely to exhibit measurable orbital motion in a reasonable time frame, and also have the best chance of eclipsing. Furthermore, there is growing evidence that a significant fraction - perhaps half - of VLM multiples are hidden in unresolved, tight systems, based on searches for radial velocity (RV) variables (e.g., Maxted & Jeffries 2005; Basri & Reiners 2006; Joergens 2008) and overluminous sources in cluster color-magnitude diagrams (e.g.,

¹For an updated list, see <http://www.vlmbinaries.org>.

Pinfield et al. 2003; Lodieu et al. 2007). Yet actual yields of very tight binaries have been small due to the inherent inefficiencies associated with these search programs: RV monitoring programs require large allocations of large telescope time, while searches for overluminous sources need clusters and long-term astrometric programs to confirm object membership. Other signatures of unresolved multiplicity, such as eclipsing (e.g., Stassun et al. 2006), astrometric wobble (e.g., Dahn et al. 2008) and microlensing (e.g., Bennett et al. 2009) have similarly yielded few detections.

We have recently developed a technique to identify and characterize a subset of VLM “spectral” binaries, or blended-light pairs, using low-resolution, near-infrared spectroscopy (Burgasser 2007b; Burgasser et al. 2008a, 2010). This technique exploits the distinct and complex structure of late-type M, L, and T dwarf near-infrared spectra as shaped by absorption bands of H_2O , CH_4 , CO , and FeH , as well as condensate cloud opacity (e.g., Reid et al. 2001; McLean et al. 2003; Cushing et al. 2005). Unresolved pairs with different component spectral types exhibit specific spectral peculiarities which arise from blended features. These peculiarities serve to both identify a source as a spectral binary and enable the decomposition of the spectrum into its component types. This technique is not limited by the angular separation of a binary, so closely-separated systems—for which dynamic mass measurements and possibly radius measurements are feasible—can potentially be identified.

An illustrative case is 2MASS J03202839–0446358 (hereafter 2MASS J0320–0446; Wilson et al. 2003), whose near-infrared spectrum exhibits an unusual absorption feature at $1.6\ \mu\text{m}$ not seen in normal M or L dwarf spectra. Burgasser et al. (2008a) were able to reproduce the spectrum of this source as the combination of an M8 primary plus T5 secondary, with the $1.6\ \mu\text{m}$ feature arising from overlapping FeH and CH_4 absorption from the two components, respectively. 2MASS J0320–0446 was independently identified as a spectroscopic binary with an 8-month orbit by Blake et al. (2008) from high-resolution spectroscopic monitoring. The inferred separation and system mass function from the Blake et al. study, and the component spectral types from the Burgasser et al. study, have enabled a firm constraint on the minimum age and component masses of 2MASS J0320–0446 ($>2\ \text{Gyr}$; $M_1 > 0.080\ M_\odot$, $M_2 > 0.053\ M_\odot$; Burgasser & Blake 2009). To date, 20 late-type M/L plus T dwarf spectral binaries have been identified in this manner (Cruz et al. 2004; Burgasser 2007b; Burgasser et al. 2008a, 2010; Looper et al. 2008a; Stumpf et al. 2008), three of which have thus far been resolved (Burgasser et al. 2006c; C. Gelino et al. 2010, in preparation).

This article reports the discovery of a new L dwarf plus T dwarf spectral binary identified from low-resolution, near-infrared spectroscopy, 2MASS J20261584–2943124 (hereafter 2MASS J2026–2943; Cruz et al. 2007). The spectrum of this source shows the distinct signature of blended FeH and CH_4 absorption, but is unresolved in high angular resolution

imaging. In Section 2 we describe our spectroscopic observations of 2MASS J2026–2943, obtained with the NASA Infrared Telescope Facility (IRTF) SpeX spectrograph (Rayner et al. 2003), and present our template fitting analysis that demonstrates the binary nature of this source and constrains its component properties. In Section 3 we describe high angular resolution images of 2MASS J2026–2943 obtained with the Keck laser guide star adaptive optics (LGS AO) system and NIRC2 camera, and present limits on the detection of the putative companion. Section 4 provides additional discussion on the properties of the putative components, and presents arguments that the system may be relatively old ($\gtrsim 5$ Gyr). Results are summarized in Section 5.

2. Near-Infrared Spectroscopy

2.1. Observations

Low resolution, near-infrared spectra for 2MASS J2026–2943 were obtained with IRTF/SpeX on three separate occasions: 2008 September 8, 2009 June 30, and 2009 November 4 (UT), as summarized in Table 1. The SpeX prism mode was used with the $0''.5$ slit for all observations, providing $0.7\text{--}2.5\ \mu\text{m}$ coverage in a single order with resolution $\lambda/\Delta\lambda \approx 120$ and dispersion of $20\text{--}30\ \text{\AA}\ \text{pixel}^{-1}$. To mitigate the effects of differential refraction, the slit was aligned to the parallactic angle in each observation. A0 V stars, either HD 186852 ($V = 8.47$) or HD 199090 ($V = 7.94$), were observed immediately after each observation of 2MASS J2026–2943 and at similar airmasses for flux calibration and telluric absorption correction. Internal flat field and argon arc lamp exposures were also obtained for pixel response and wavelength calibration. Data were reduced with the SpeXtool package, version 3.4 (Vacca et al. 2003; Cushing et al. 2004), using standard settings. A detailed description of the reduction procedures is given in Burgasser (2007b).

2.2. The Near-Infrared Spectrum of 2MASS J2026–2943

Reduced spectral data of 2MASS J2026–2943 from all three epochs are shown in Figure 1, compared to equivalent data for the L1 spectral standard 2MASS J14392836+1929149 (hereafter 2MASS J1439+1929; Kirkpatrick et al. 1999) and 2MASS J0320–0446. Overall, the near-infrared spectral morphology of 2MASS J2026–2943 is similar to these sources and other late-type M and early-type L dwarfs, with TiO absorption at red optical wavelengths (0.76 and $0.85\ \mu\text{m}$); prominent H_2O absorption at 1.4 and $1.8\ \mu\text{m}$; FeH absorption at 0.99 , 1.2 , and $1.55\ \mu\text{m}$; unresolved Na I and K I doublet line absorption in the $1.0\text{--}1.3\ \mu\text{m}$ region

and at $2.2\ \mu\text{m}$; and CO bandheads at $2.3\text{--}2.4\ \mu\text{m}$. 2MASS J2026–2943 has a somewhat redder spectrum than 2MASS J0320–0446 and 2MASS J1439+1929, consistent with its redder $J - K_s$ color (1.44 ± 0.05 versus 1.13 ± 0.04 and 1.21 ± 0.03 , respectively). It also exhibits a somewhat more pronounced $1.27\ \mu\text{m}$ flux peak. All three epochs of spectral data of 2MASS J2026–2943 are generally consistent with each other, differing by less than $\pm 5\%$ across the $0.85\text{--}2.4\ \mu\text{m}$ range.

The one striking feature in the near-infrared spectrum of 2MASS J2026–2943 is the sharp dip at $1.6\ \mu\text{m}$, also seen in the spectrum of 2MASS J0320–0446 but not 2MASS J1439+1929. This feature is nearly coincident with the $1.57\text{--}1.64\ \mu\text{m}$ FeH absorption band but has a different morphology, forming more of a wedge-shaped divet in contradistinction to the flat plateau in the spectrum of 2MASS J1439+1929. This feature is present in all three epochs of spectral data. As discussed in Burgasser (2007b), this feature can arise in the combined-light spectrum of a late-type M/L dwarf plus T dwarf binary, where FeH absorption in the spectrum of the former overlaps with CH_4 absorption in the spectrum of the latter, resulting in a hybrid feature with this particular shape. The presence of the $1.6\ \mu\text{m}$ dip therefore signifies 2MASS J2026–2943 as a potential unresolved binary system.

2.3. Spectral Template Analysis

2.3.1. Template Sample

To assess the likelihood of 2MASS J2026–2943 being a binary, we applied the spectral template comparison technique described in detail in Burgasser et al. (2010). A total of 437 SpeX prism spectra of 415 M7–T8 dwarfs were drawn from the SpeX Prism Spectral Libraries² and our own observations. These spectra were required to have median signal-to-noise ratios of 20 or greater over the $0.9\text{--}2.4\ \mu\text{m}$ window, and we explicitly excluded known binaries, young cluster objects (e.g., Muench et al. 2007), and sources specifically noted to have peculiar spectra associated with low surface gravities, subsolar metallicities, unusual cloud properties or highly uncertain spectral types (e.g.; Knapp et al. 2004; Chiu et al. 2006; Cruz et al. 2007, 2009; Burgasser et al. 2008b;Looper et al. 2008b).

²<http://www.browndwarfs.org/spexprism>. Data were drawn specifically from Burgasser et al. (2004, 2006a,b, 2007a, 2008a,b); Cruz et al. (2004); Burgasser & McElwain (2006); Chiu et al. (2006); McElwain & Burgasser (2006); Reid et al. (2006); Burgasser (2007a,b,c); Liebert & Burgasser (2007); Looper et al. (2007, 2008b); Luhman et al. (2007b); Siegler et al. (2007); Sheppard & Cushing (2009); and Burgasser et al. (2010).

These spectra were interpolated onto a common wavelength scale and flux-calibrated into absolute flux units (F_λ at 10 pc) using a combination of the 2MASS M_J /spectral type relation from Cruz et al. (2003) for M7–L2 dwarfs and the 2MASS M_{K_s} /spectral type relation from Looper et al. (2008a) for L2–T8 dwarfs. Spectrophotometric magnitudes were computed directly from the SpeX spectra by integrating these and a Kurucz model spectrum of Vega with the 2MASS filter profiles (see Cushing et al. 2005). Spectral types were culled from the literature,³ with optical classifications used for M7–L8 dwarfs (tied to the schemes of Kirkpatrick et al. 1991 and Kirkpatrick et al. 1999) and near-infrared classifications used for L9–T8 dwarfs (tied to the scheme of Burgasser et al. 2006b) and any M or L dwarf without a published optical classification (based on various schemes: Reid et al. 2001; Testi et al. 2001; McLean et al. 2003; Nakajima et al. 2004; Burgasser 2007a).

From these flux-calibrated spectra, 99,467 combined-light binary spectral templates were constructed by adding together all possible pairs that satisfied the requirement that one spectrum (the secondary) was of equal or later spectral type than the other (the primary).

2.3.2. Template Comparison

Each spectrum of 2MASS J2026–2943 was compared to the single and binary templates to identify best-fit matches. All spectra were initially normalized to the maximum flux in the 1.2–1.3 μm region. We then computed the chi-square difference statistic between each spectrum of 2MASS J2026–2943 ($S[\lambda]$) and each template spectrum ($T[\lambda]$):

$$\chi^2 \equiv \sum_{\{\lambda\}} \left[\frac{S[\lambda] - \alpha T[\lambda]}{\sigma_c[\lambda]} \right]^2. \quad (1)$$

Here, α is a scaling factor that minimizes χ^2 (see Equation 2 in Cushing et al. 2008), $\sigma_c[\lambda]$ is the noise spectrum of 2MASS J2026–2943, and the sum is performed over the wavelength ranges $\{\lambda\} = 0.95\text{--}1.35 \mu\text{m}$, $1.45\text{--}1.8 \mu\text{m}$ and $2.0\text{--}2.35 \mu\text{m}$ in order to avoid regions of strong telluric absorption. Unlike Burgasser et al. (2010), we did not use a weighting scheme so each spectral pixel has equal weight in the fit.

Because we are comparing the spectra of distinct sources rather than an optimized spectral model, our expectation is not to achieve $\chi^2 \approx 1$ for our best-fit cases. Rather, we wish to assess whether any binary templates provide significantly better fits to the spectra of 2MASS J2026–2943 than the best-fit single template. As the number of binary templates

³As compiled at <http://dwarfarchives.org>.

vastly outnumbers the number of single templates, a better fit (lower χ^2) is almost assured so it is necessary to assess the statistical significance of improvement. As in Burgasser et al. (2010), we used the one-sided F-test for this purpose, using as our distribution statistic the ratio

$$\eta_{SB} \equiv \frac{\min(\{\chi_{single}^2\})/\nu_{single}}{\min(\{\chi_{binary}^2\})/\nu_{binary}} \quad (2)$$

where $\nu_{single} = \nu_{binary} \equiv \nu = 211$ is the degrees of freedom in each fit, equal to the number of data points minus one to account for the relative scaling (α) between 2MASS J2026–2943 and each template spectrum. To rule out the null hypothesis—that 2MASS J2026–2943 is not a binary—at the 99% confidence level (CL), we required $\eta_{SB} > 1.34$.

Finally, since multiple single and binary templates yield χ^2 values that are statistically indistinct from each other, we computed mean values and uncertainties for the component parameters (i.e., spectral types and relative brightnesses) using a weighting scheme based on the F-distribution:

$$W_i \propto 1 - F(\eta_{i0} \mid \nu, \nu). \quad (3)$$

Here, $\eta_{i0} \equiv \chi_{i0}^2/\min([\chi^2])$ is the ratio of chi-square residuals between the best-fit template and the i^{th} template, and $F(\eta_{i0} \mid \nu, \nu)$ is the F-distribution probability distribution function. Parameter means (\bar{p}) and uncertainties (σ_p) were computed as

$$\bar{p} \equiv \frac{\sum_i W_i p_i}{\sum_i W_i} \quad (4)$$

and

$$\sigma_p^2 = \frac{\sum_i W_i (p_i - \bar{p})^2}{\sum_i W_i}. \quad (5)$$

2.4. Results

The best-fitting single and binary spectral templates to the data for 2MASS J2026–2943 are shown Figure 2, and component parameters are listed in Table 2. For each observation, a combined-light spectrum composed of a late-type M/early-type L dwarf primary and mid-type T dwarf secondary provides a statistically significant better match to the spectrum of 2MASS J2026–2943 than the best-fit single template, with confidence levels >99.9% in all three cases. More importantly, the binary templates consistently reproduce the 1.6 μm feature, with the T dwarf secondary contributing roughly 5% to the pseudo-continuum shortward of this feature. The addition of a T dwarf secondary also explains the strong 1.27 μm peak in the spectrum of 2MASS J2026–2943, contributing up to 10% of the flux between strong H₂O and CH₄ bands. Overall, however, the T dwarf secondary contributes minimally

to combined-light spectrum; mean relative JHK magnitudes on the MKO⁴ system range over $\Delta J = 3.0\text{--}3.5$, $\Delta H = 4.0\text{--}4.5$ and $\Delta K = 4.5\text{--}5.2$.

The mean component parameters for the three observations of 2MASS J2026–2943 are in fairly good agreement with each other, with the first two spectra indicating an L1 primary and a T5.5–T6.5 secondary, a somewhat later-type combination than 2MASS J0320–0446 (M8.5+T5; Burgasser et al. 2008a). The 2009 Nov 4 spectrum, however, indicates somewhat earlier-type primary and secondary components, M9.5 + T4.5, although the uncertainty on the latter is much higher. The estimated relative magnitudes are all in agreement, due in part to their large uncertainties ($\pm 0.2\text{--}0.4$ for ΔJ to $\pm 1.5\text{--}1.8$ for ΔK). Uncertainty-weighted means and uncertainties for these parameters based on all three observations are listed in Table 3.

3. LGS AO Imaging

3.1. Observations

In an attempt to identify the faint companion inferred from the spectral analysis, 2MASS J2026–2943 was imaged on 2009 August 15 (UT) with the sodium LGS AO system (Wizinowich et al. 2006; van Dam et al. 2006) and facility near-infrared camera NIRC2 on the 10m Keck II Telescope. Conditions were fair with clear skies and below average seeing ($\sim 1''$). The narrow field-of-view camera of NIRC2 was utilized, providing an image scale of 9.963 ± 0.011 mas/pixel (Pravdo et al. 2006) over a $10.2'' \times 10.2''$ field of view with no rotation. Observations were conducted through the MKO J , H , and K_s -band filters. For each filter we employed a simple 3-position dither pattern that avoided the noisy, lower left quadrant of the focal plane array. Exposure times at each dither position are listed in Table 1. The LGS provided the wavefront reference source for AO correction, while tip-tilt aberrations and quasi-static changes were measured contemporaneously by monitoring the $R = 13.3$ mag field star USNO 0602-0932082 (Monet et al. 2003), located $44''$ away from 2MASS J2026–2943. We also obtained observations of the nearby star 2MASS J20282802–2844422 ($H = 13.01$ mag) in the H -band as a point spread function (PSF) calibrator, using the $R = 12.9$ mag field star USNO 0612-0905762 ($\rho = 43''$) for tip-tilt correction. Because the PSF of LGS-AO images are known to be highly variable based on the brightness of the tip-tilt reference star, the vector (distance and position angle) to the tip-tilt star, and atmospheric effects (airmass, seeing, etc.), the properties of the tip-tilt star for the PSF calibrator are chosen to be as

⁴Mauna Kea Observatory filter system; see Tokunaga et al. (2002) and Simons & Tokunaga (2002).

similar as possible to the properties of the tip-tilt star used for the target.

Images were reduced using custom scripts. Sky frames, obtained by the median average of the 3 dithered target exposures, were subtracted from each image. A dome flat was used to correct for pixel-to-pixel sensitivity differences. The three images were then registered to the peak of the target’s PSF, and median combined to produce the final stacked images shown in Figure 3. No further astrometric or photometric calibration was performed on the final stacked image.

3.2. Limits on the Presence of a Faint Companion

Initial examination of the AO images showed no discernible companion to 2MASS J2026–2943 within $3''$ of its peak brightness in any of the three bands. A second source is detected in the field at a separation of $3.6''$ and position angle 254° which is $\Delta H \approx 4.5$ mag fainter, comparable to the predicted relative brightness of the expected companion. However, this source is too widely separated to have fallen in the slit with 2MASS J2026–2943 in the SpeX spectral observations, and as such could not have contributed to the spectrum shown in Figure 1. It is also too wide to have been coincident with 2MASS J2026–2943 at the time of the SpeX observations, based on the latter’s measured proper motion (350 ± 15 mas yr $^{-1}$; Jameson et al. 2008). A second epoch observation of the 2MASS J2026–2943 field would determine if the faint detected source is physically bound to 2MASS J2026–2943; however, current evidence indicates that it is an unrelated background source. No other sources are detected in the field with a $\Delta H < 7$ mag (the $10\text{-}\sigma$ limit).

A better limit on the presence of a close companion to 2MASS J2026–2943 was made from PSF subtraction. Figure 4 compares the PSF of 2MASS J2026–2943 to that of the PSF star 2MASS J20282802–2844422 at H -band, as well as the resulting PSF-subtracted image. While the calibrator PSF is not a perfect match to that of 2MASS J2026–2943, the benefits for reducing the halo of 2MASS J2026–2943 are quite evident. At $0''.25$ the flux from the primary’s halo is reduced by a factor of 10, thus facilitating the detection of companions at the expected brightness of the secondary beyond that separation. However, no companions are seen.

To quantify our detection limits, we generated a set of 10,000 synthetic H -band images of the 2MASS J2026–2943 field with implanted companion sources. These “false” companions were reproductions of the 2MASS J2026–2943 PSF, scaled to the expected magnitude difference of the putative companion ($\Delta H = 4.2$ mag) and inserted at random positions over radial distances spanning 0–100 pixels ($0\text{--}1''$) and all position angles. Each of the 10,000 synthetic

companions were placed on both the original source image and the PSF-subtracted image. We used the SExtractor program (Bertin & Arnouts 1996) to automatically search for the planted companions. A detection was considered “good” if there was a point source found within 2 pixels of the known location of the planted companion. These detections were also visually examined to assess the reliability of the SExtractor detection algorithm, which generally did a comparable job of finding companions as visual inspection albeit with somewhat less reliability within $0''.25$. Therefore, we consider the SExtractor results to be a conservative upper limit for the maximum detectable separation of a binary 2MASS J2026–2943.

Figure 5 shows the ratio of detections to non-detections as a function of radial distance, based on bins 5 pixels in width. As expected, the planted companions were detected at closer distances in the PSF-subtracted image compared to the non-PSF-subtracted image (Figure 5), and our reported limit is based on the former. This analysis indicates that a source with a relative brightness as predicted from the spectral template matching results should have been detected $\gtrsim 50\%$ of the time at separations beyond $0''.25$. This is also where visual inspection begins to find the majority of the planted companions. We therefore adopt $0''.25$ as the maximum angular separation of the companion at the epoch of observation, which corresponds to a projected separation limit of 9 AU at the estimated distance of this source (36 ± 5 pc; Cruz et al. 2007). Note that this is not a particularly restrictive limit; it falls above the peak of the VLM binary separation distribution ($7.2^{+1.1}_{-1.7}$ AU for a logarithmic distribution; Allen 2007), and only 25% of known VLM binaries have projected separations wider than 9 AU.

4. Discussion

The predicted properties of the putative 2MASS J2026–2943 binary are summarized in Table 3. The luminosities of the components, based on their inferred spectral types and the M_{bol} /spectral type relation of Burgasser (2007a), are $\log_{10} L_{bol}/L_{\odot} = -3.64 \pm 0.10$ and -5.1 ± 0.2 , corresponding to masses of $0.077 M_{\odot}$ and $0.030 M_{\odot}$ ($0.084 M_{\odot}$ and $0.072 M_{\odot}$) for an age of 1 Gyr (10 Gyr), based on the evolutionary models of Burrows et al. (1997). With these parameters, the separation limit of the secondary corresponds to an orbital period of 82 yr (68 yr) and a primary radial velocity (RV) variation amplitude of 27 m s^{-1} (42 m s^{-1}), assuming an edge-on circular orbit contained within 9 AU. This RV amplitude is well below the $\approx 320 \text{ m s}^{-1}$ systematic uncertainties found by Blake et al. (2008) for their observations of 2MASS J0320–0446, and the $200\text{--}300 \text{ m s}^{-1}$ uncertainty found by Zapatero Osorio et al. (2009) and Konopacky et al. (2010) in comparable near-infrared observations of other VLM sources. However, if the 2MASS J2026–2943 system is more closely separated than the AO

limits indicate—and older—there is a reasonable chance of measuring RV variability in this system in a viable timescale. For example, for an edge-on orbit with separation of 1 AU and system age of 5 Gyr, the 2MASS J2026–2943 primary would exhibit a 2.5 yr, 240 m s^{−1} peak-to-peak RV variation, potentially detectable with current instrumentation.

There are several lines of evidence that suggest that 2MASS J2026–2943 is a relatively old VLM system. The optical spectrum of the primary from Cruz et al. (2007) shows no evidence for the 6708 Å Li I absorption line, indicating a minimum mass for this component of 0.06 M_⊙ (Chabrier & Baraffe 1997; Ushomirsky et al. 1998) and a minimum age of 0.4 Gyr (Burrows et al. 1997). This spectrum also shows no discernible Hα emission, a feature commonly observed in younger, more magnetically active late-type M and L dwarfs (e.g., Schmidt et al. 2007; West et al. 2008). The proper motion of 2MASS J2026–2943 indicates a tangential velocity ($V_{tan} = 60 \pm 9$ km s^{−1}) that is more than 1 sigma faster than the 20 pc sample of L0-L9 dwarfs from (Faherty et al. 2009). Given the inferred age of that sample ($3.2^{+1.1}_{-0.9}$ Gyr), the age of 2MASS J2026–2943 can be estimated to be at least 3 Gyr, but more likely older. Finally, the binary nature of 2MASS J2026–2943 and properties of its components also suggest an older age. The majority of VLM binaries are found in near-equal mass systems, $q \equiv M_2/M_1 \approx 1$ (Bouy et al. 2003; Burgasser et al. 2003; Allen 2007). Although many imaging surveys are sensitive to mass ratios below ~ 0.4 for separations smaller than 0".2 (e.g., Burgasser et al. 2006c), roughly 80% of known VLM pairs have $q \gtrsim 0.75$. Based on the inferred masses of its components, the 2MASS J2026–2943 system would have to have an age $\gtrsim 5$ Gyr to follow the same trend. Direct mass measurements of the components, perhaps through the detection of RV variations, would provide a more precise constraint on the age of this system, as has been demonstrated for 2MASS J0320–0446 (Burgasser & Blake 2009).

5. Conclusions

We have identified 2MASS J2026–2943 as a L0.5 plus T6 spectral binary, based on the presence of a peculiar 1.6 μm feature in its near-infrared spectrum. We associate this feature with overlapping FeH and CH₄ absorption from the primary and secondary, respectively. LGS AO imaging failed to resolve a companion to a minimum separation limit of 0".25, or 9 AU in projected separation, a fairly unrestrictive limit given the properties of VLM binaries at large. The inability to resolve this pair may be due in part to the large inferred magnitude difference of its components; its predicted $\Delta H = 4.2 \pm 0.6$ mag is comparable to the largest relative magnitudes measured for any VLM pair (e.g., 2MASS J1207334–393254AB, $\Delta H \approx 5.6$; Chauvin et al. 2004; GJ 802AB, $\Delta H \approx 4.7$; Lloyd et al. 2006; SCR J1845–6357, $\Delta H \approx$

4.2; Biller et al. 2006). Alternately, 2MASS J2026–2943, like 2MASS J0320–0446, may be a very tightly bound system, raising the distinct possibility that direct mass measurements via astrometric and/or radial velocity orbital monitoring are viable. As few direct mass measurements are currently available for VLM stars and brown dwarfs, additional follow-up observations—e.g., LGS AO aperture masking observations (Tuthill et al. 2006) or high resolution spectroscopic monitoring—to resolve this system and/or measure the properties of its components is warranted. 2MASS J2026–2943 joins a growing list of unresolved, VLM binary candidates whose inferred components straddle the two lowest-luminosity classes of stars and brown dwarfs.

The authors acknowledge telescope operators Bill Golisch, Paul Sears and Eric Volquardsen, and instrument specialist John Rayner at IRTF; and Hien Tran and Jason McIlroy at Keck, for their assistance during the observations. We also wish to thank the referee, Kevin Luhman, for his very prompt and helpful review. This publication makes use of data from the Two Micron All Sky Survey, which is a joint project of the University of Massachusetts and the Infrared Processing and Analysis Center, and funded by the National Aeronautics and Space Administration and the National Science Foundation. 2MASS data were obtained from the NASA/IPAC Infrared Science Archive, which is operated by the Jet Propulsion Laboratory, California Institute of Technology, under contract with the National Aeronautics and Space Administration. This research has benefitted from the M, L, and T dwarf compendium housed at <http://DwarfArchives.org> and maintained by Chris Gelino, Davy Kirkpatrick, and Adam Burgasser; the Very-Low-Mass Binaries Archive housed at <http://www.vlmbinaries.org> and maintained by Nick Siegler, Chris Gelino, and Adam Burgasser; and the SpeX Prism Spectral Libraries, maintained by Adam Burgasser at <http://www.browndwarfs.org/spexprism>. The authors recognize and acknowledge the very significant cultural role and reverence that the summit of Mauna Kea has always had within the indigenous Hawaiian community. We are most fortunate to have the opportunity to conduct observations from this mountain.

Facilities: IRTF (SpeX), Keck (NIRC2,LGS)

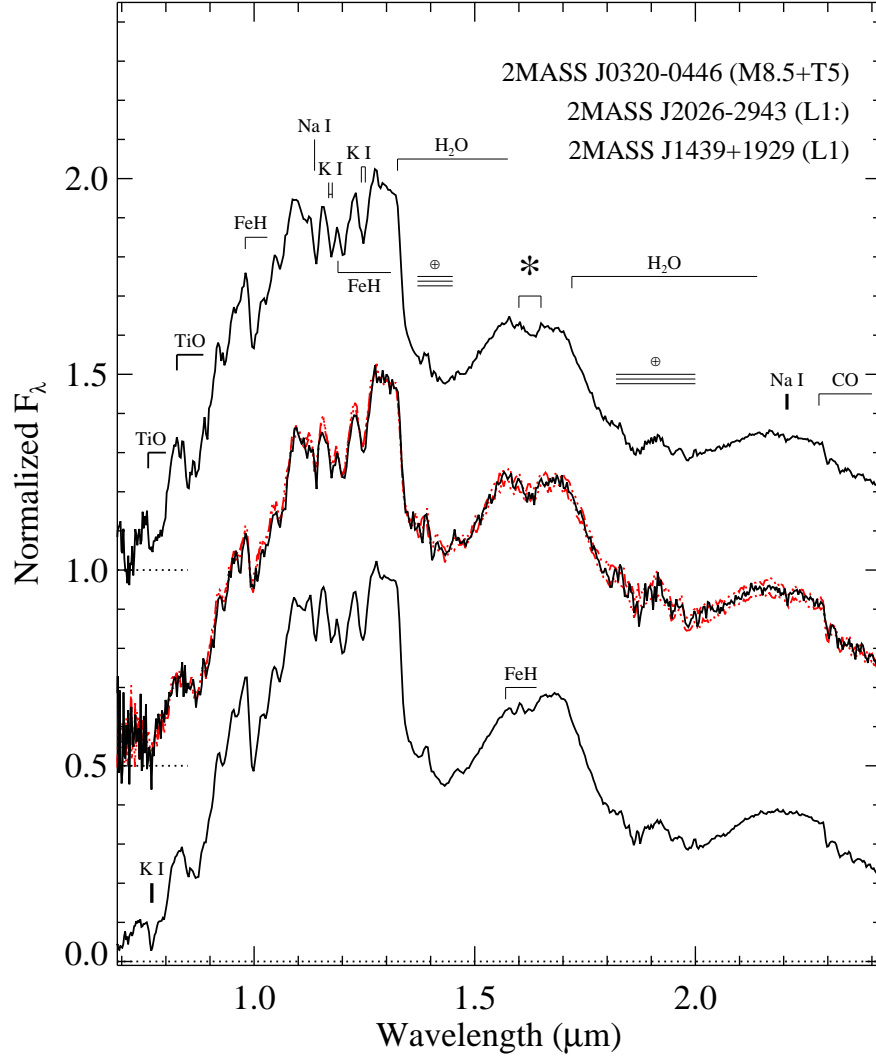


Fig. 1.— SpeX prism spectrum of 2MASS J2026–2943 (center: black line from 2009 June 30 UT; red lines from 2008 September 8 UT and 2009 November 4 UT) compared to equivalent data for the M8.5+T5 spectral binary 2MASS J0320–0446 (top; data from Burgasser et al. 2008a) and the L1 spectral standard 2MASS J1439+1929 (bottom; data from Burgasser et al. 2004). All three spectra are normalized at $1.25\ \mu\text{m}$ and offset by constants (dotted lines). Prominent features resolved by these spectra are indicated. The peculiar $1.6\ \mu\text{m}$ feature in the spectra of 2MASS J0320–0446 and 2MASS J2026–2943 as discussed in the text is indicated by an asterisk.

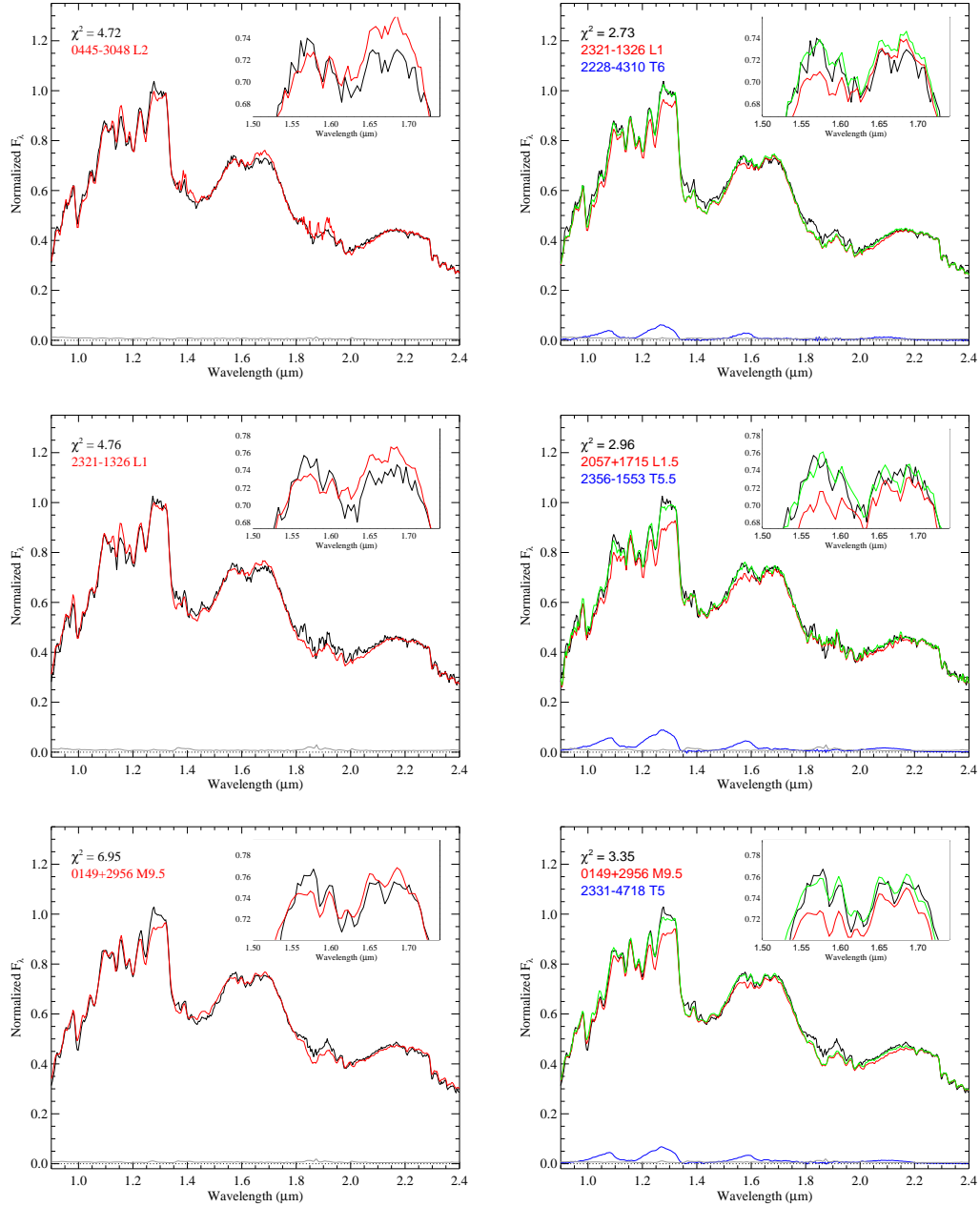


Fig. 2.— (Left): The best-fit single spectral templates (red lines) to the three epochs of spectral data for 2MASS J2026–2943 (black lines), from top to bottom: 2008 September 8, 2009 June 30 and 2009 November 4 (UT). (Right): The best-fit binary spectral templates (green lines), and component primaries (red lines) and secondaries (blue lines) for the same epochs. All spectra are normalized in the 1.2–1.3 μm region, with the single and binary templates scaled to minimize their χ^2 deviations. The primary and secondary component spectra in the bottom panel are scaled according to their contribution to the binary templates. Inset boxes show a close-up of the 1.5–1.75 μm region where the peculiar 1.6 μm feature is located.

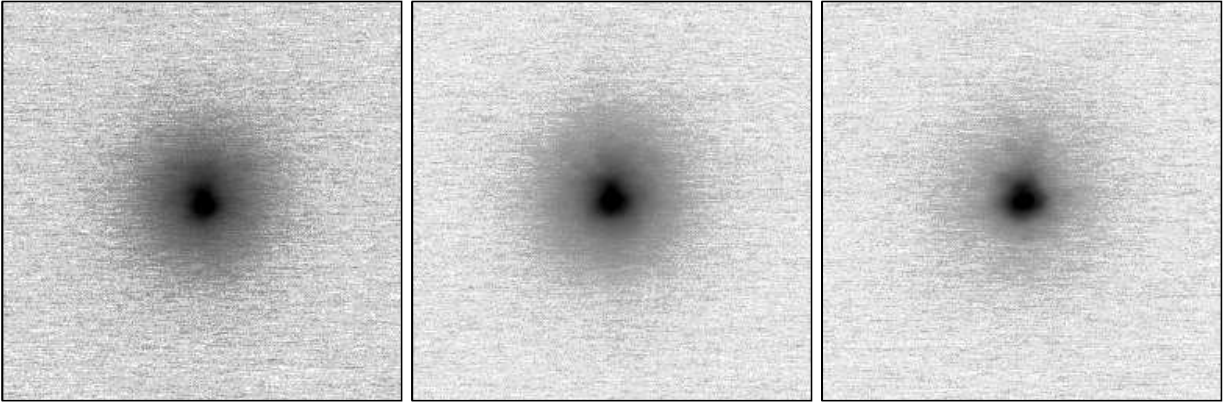


Fig. 3.— J, H, K_s Keck NIRC2/LGS AO images of 2MASS J2026–2943 from 2009 August 15 (UT). The images are $2''.5$ on a side and oriented with North up and East to the left. The full-width half maxima and Strehl ratios for the final images are 81mas and 1.4% for J , 83mas and 4.9% for H , and 84mas and 12% for K_s .

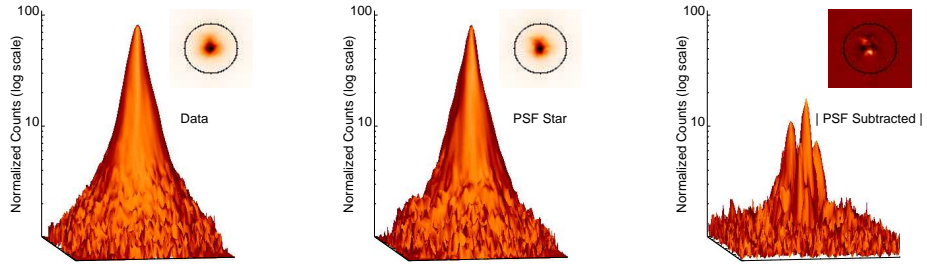


Fig. 4.— PSF-fitting to H -band imaging data for 2MASS J2026–2943. Shown are the normalized surface fluxes on a logarithmic scale and images on a linear scale (inset boxes) for $0''.8 \times 0''.8$ regions around the source (left), the PSF calibrator star (middle) and the PSF-subtracted residuals (absolute values) as scaled to the original data (right). Maximum residuals are roughly 20% of the peak source flux. The $0''.25$ radius region around the source position beyond which a companion can be ruled out is indicated in the inset images. At the displayed scaling, the inferred secondary of this system would have a peak flux of roughly 2.

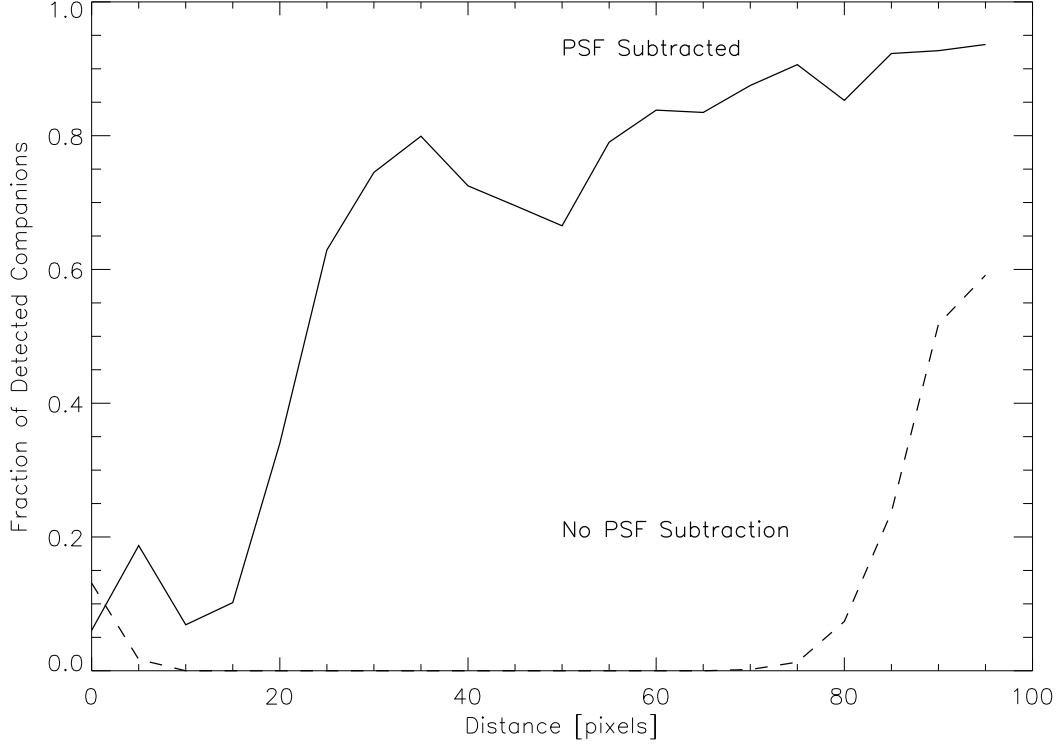


Fig. 5.— The probability of detecting a companion to 2MASS J2026–2943 comparable in brightness to that inferred from the spectral analysis in the PSF-subtracted (solid line) and non-PSF-subtracted (dashed line) images. The benefits of using PSF subtraction for companion detection at small radial distances is clearly evident in the greatly enhanced fraction of detected companions closer than 80 pixels ($\approx 0''.8$). We adopt a minimum companion detection limit of $0''.25$, where the probability of detection rises above 50%.

Table 1. Observations of 2MASS J2026–2943.

| Instrument | Date | Setup | Integration | Airmass | Conditions |
|--------------------|-------------|-----------------------|-------------|---------|---------------------------|
| IRTF/SpeX | 2008 Sep 8 | 0''5 slit, prism mode | 150s×6 | 1.54 | clear, 1'' seeing |
| IRTF/SpeX | 2009 Jun 30 | 0''5 slit, prism mode | 120s×8 | 1.54 | clear, 1'' seeing |
| IRTF/SpeX | 2009 Nov 4 | 0''5 slit, prism mode | 150s×8 | 1.60 | light cirrus, 0''5 seeing |
| Keck/NIRC2 + LGSAO | 2009 Aug 15 | J , narrow camera | 60s×4 | 1.58 | clear, 1'' seeing, RH~20% |
| Keck/NIRC2 + LGSAO | 2009 Aug 15 | H , narrow camera | 30s×6 | 1.54 | ... |
| Keck/NIRC2 + LGSAO | 2009 Aug 15 | K_s , narrow camera | 15s×16 | 1.55 | ... |

Table 2. Spectral Template Fits.

| Primary | SpT | Secondary | SpT | ΔJ | ΔH | ΔK | χ^2/CL |
|-------------------------|----------|-------------------------|----------|------------|------------|------------|--------------------|
| 2008 Sep 8 | | | | | | | |
| 2MASS J0445538-304820 | L2 | ... | ... | ... | ... | ... | 4.72 |
| 2MASS J23211254-1326282 | L1 | 2MASS J22282889-4310262 | T6 | 3.37 | 4.39 | 4.85 | 2.73 |
| <Primary> | L1.2±0.5 | <Secondary> | T6.5±0.7 | 3.5±0.4 | 4.5±1.1 | 5.2±1.8 | 99.996% |
| 2009 Jun 30 | | | | | | | |
| 2MASS J23211254-1326282 | L1 | ... | ... | ... | ... | ... | 4.76 |
| 2MASS J2057153+171515 | L1.5 | 2MASS J2356547-155310 | T5.5 | 2.85 | 3.83 | 4.39 | 2.96 |
| <Primary> | L0.8±0.9 | <Secondary> | T5.5±0.6 | 3.0±0.2 | 4.0±1.1 | 4.6±1.7 | 99.971% |
| 2009 Nov 4 | | | | | | | |
| 2MASS J01490895+2956131 | M9.5 | ... | ... | ... | ... | ... | 6.95 |
| 2MASS J01490895+2956131 | M9.5 | 2MASS J23312378-4718274 | T5 | 3.23 | 4.08 | 4.60 | 3.35 |
| <Primary> | M9.5±0.0 | <Secondary> | T4.7±1.2 | 3.2±0.3 | 4.0±1.0 | 4.5±1.5 | 99.999% |

Table 3. Component and System Parameters for 2MASS J2026–2943.

| Parameter | 2MASS J2026–2943A | 2MASS J2026–2943B | Difference | Ref |
|---|-------------------|-------------------|-------------------|-----|
| Spectral Type | L0.5 | T6.0 | ... | 1 |
| J^a (mag) | 14.86±0.03 | 17.98±0.15 | 3.12±0.16 | 1 |
| H^a (mag) | 13.97±0.03 | 18.2±0.6 | 4.2±0.6 | 1 |
| K^a (mag) | 13.37±0.04 | 18.1±1.0 | 4.7±1.0 | 1 |
| $\log_{10} L_{bol}/L_{\odot}^b$ | -3.64±0.10 | -5.1±0.2 | 1.5±0.3 | 1,2 |
| d (pc) | 36±5 | ... | ... | 3 |
| μ (mas/yr) | 351±15 | ... | ... | 4 |
| V_{tan} (km s ⁻¹) | 66±7 | ... | ... | 3,4 |
| ρ (AU) | <0''.25 (<9 AU) | | ... | 1,3 |
| Mass ^c (M _⊙) at 1 Gyr | 0.077 | 0.030 | 0.39 ^d | 5 |
| Mass ^c (M _⊙) at 5 Gyr | 0.084 | 0.063 | 0.75 ^d | 5 |
| Mass ^c (M _⊙) at 10 Gyr | 0.084 | 0.072 | 0.86 ^d | 5 |

^aSynthetic magnitudes on the MKO system, based on 2MASS JHK_s photometry for the unresolved source and spectrophotometry of the binary template components.

^bBased on the M_{bol} /spectral type relation of Burgasser (2007a).

^cBased on evolutionary models from Burrows et al. (1997) and estimated luminosities.

^dMass ratio $q \equiv M_2/M_1$.

References. — (1) This paper; (2) Burgasser (2007a); (3) Cruz et al. (2007); (4) Jameson et al. (2008); (5) Burrows et al. (1997).

REFERENCES

- Allen, P. R. 2007, *ApJ*, 668, 492
- Basri, G., & Martín, E. L. 1999, *AJ*, 118, 2460
- Basri, G., & Reiners, A. 2006, *AJ*, 132, 663
- Bennett, D. P., Rhie, S. H., Nikolaev, S., Gaudi, B. S., Udalski, A., Gould, A., Christie, G. W., Maoz, D., Dong, S., McCormick, J., Szymanski, M. K., Tristram, P. J., Macintosh, B., Cook, K. H., Kubiak, M., Pietrzynski, G., Soszynski, I., Szewczyk, O., Ulaczyk, K., Wyrzykowski, L., DePoy, D. L., Han, C., Kaspi, S., Lee, C. -, Mallia, F., Natusch, T., Park, B. -, Pogge, R. W., Polishook, D., Abe, F., Bond, I. A., Botzler, C. S., Fukui, A., Hearnshaw, J. B., Itow, Y., Kamiya, K., Korpela, A. V., Kilmartin, P. M., Lin, W., Masuda, K., Matsubara, Y., Motomura, M., Muraki, Y., Nakamura, S., Okumura, T., Ohnishi, K., Perrott, Y. C., Rattenbury, N. J., Sako, T., Saito, T., Sato, S., Skuljan, L., Sullivan, D. J., Sumi, T., Sweatman, W. L., Yock, P. C. M., Albrow, M., Allan, A., Beaulieu, J. -, Bramich, D. M., Burgdorf, M. J., Coutures, C., Dominik, M., Dieters, S., Fouque, P., Greenhill, J., Horne, K., Snodgrass, C., Steele, I., Tsapras, Y., Chaboyer, B., Crocker, A., & Frank, S. 2009, *ArXiv e-prints*
- Bertin, E., & Arnouts, S. 1996, *A&AS*, 117, 393
- Biller, B. A., Kasper, M., Close, L. M., Brandner, W., & Kellner, S. 2006, *ApJ*, 641, L141
- Blake, C. H., Charbonneau, D., White, R. J., Torres, G., Marley, M. S., & Saumon, D. 2008, *ApJ*, 678, L125
- Bouy, H., Brandner, W., Martín, E. L., Delfosse, X., Allard, F., & Basri, G. 2003, *AJ*, 126, 1526
- Burgasser, A. J. 2007a, *ApJ*, 659, 655
- . 2007b, *AJ*, 134, 1330
- . 2007c, *ApJ*, 658, 617
- Burgasser, A. J., & Blake, C. H. 2009, *AJ*, 137, 4621
- Burgasser, A. J., Burrows, A., & Kirkpatrick, J. D. 2006a, *ApJ*, 639, 1095
- Burgasser, A. J., Cruz, K. L., Cushing, M., Gelino, C. R., Looper, D. L., Faherty, J. K., Kirkpatrick, J. D., & Reid, I. N. 2010, *ApJ*, 710, 1142

- Burgasser, A. J., Geballe, T. R., Leggett, S. K., Kirkpatrick, J. D., & Golimowski, D. A. 2006b, *ApJ*, 637, 1067
- Burgasser, A. J., Kirkpatrick, J. D., Cruz, K. L., Reid, I. N., Leggett, S. K., Liebert, J., Burrows, A., & Brown, M. E. 2006c, *ApJS*, 166, 585
- Burgasser, A. J., Kirkpatrick, J. D., Reid, I. N., Brown, M. E., Miskey, C. L., & Gizis, J. E. 2003, *ApJ*, 586, 512
- Burgasser, A. J., Liu, M. C., Ireland, M. J., Cruz, K. L., & Dupuy, T. J. 2008a, *ApJ*, 681, 579
- Burgasser, A. J., Looper, D. L., Kirkpatrick, J. D., Cruz, K. L., & Swift, B. J. 2008b, *ApJ*, 674, 451
- Burgasser, A. J., Looper, D. L., Kirkpatrick, J. D., & Liu, M. C. 2007a, *ApJ*, 658, 557
- Burgasser, A. J., & McElwain, M. W. 2006, *AJ*, 131, 1007
- Burgasser, A. J., McElwain, M. W., Kirkpatrick, J. D., Cruz, K. L., Tinney, C. G., & Reid, I. N. 2004, *AJ*, 127, 2856
- Burgasser, A. J., Reid, I. N., Siegler, N., Close, L., Allen, P., Lowrance, P., & Gizis, J. 2007b, *Protostars and Planets V*, 427
- Burrows, A., Marley, M., Hubbard, W. B., Lunine, J. I., Guillot, T., Saumon, D., Freedman, R., Sudarsky, D., & Sharp, C. 1997, *ApJ*, 491, 856
- Burrows, A., Sudarsky, D., & Hubeny, I. 2006, *ApJ*, 640, 1063
- Chabrier, G., & Baraffe, I. 1997, *A&A*, 327, 1039
- Chauvin, G., Lagrange, A.-M., Dumas, C., Zuckerman, B., Mouillet, D., Song, I., Beuzit, J.-L., & Lowrance, P. 2004, *A&A*, 425, L29
- Chiu, K., Fan, X., Leggett, S. K., Golimowski, D. A., Zheng, W., Geballe, T. R., Schneider, D. P., & Brinkmann, J. 2006, *AJ*, 131, 2722
- Cruz, K. L., Burgasser, A. J., Reid, I. N., & Liebert, J. 2004, *ApJ*, 604, L61
- Cruz, K. L., Kirkpatrick, J. D., & Burgasser, A. J. 2009, *AJ*, 137, 3345
- Cruz, K. L., Reid, I. N., Kirkpatrick, J. D., Burgasser, A. J., Liebert, J., Solomon, A. R., Schmidt, S. J., Allen, P. R., Hawley, S. L., & Covey, K. R. 2007, *AJ*, 133, 439

- Cruz, K. L., Reid, I. N., Liebert, J., Kirkpatrick, J. D., & Lowrance, P. J. 2003, *AJ*, 126, 2421
- Cushing, M. C., Marley, M. S., Saumon, D., Kelly, B. C., Vacca, W. D., Rayner, J. T., Freedman, R. S., Lodders, K., & Roellig, T. L. 2008, *ApJ*, 678, 1372
- Cushing, M. C., Rayner, J. T., & Vacca, W. D. 2005, *ApJ*, 623, 1115
- Cushing, M. C., Vacca, W. D., & Rayner, J. T. 2004, *PASP*, 116, 362
- Dahn, C. C., Harris, H. C., Vrba, F. J., Guetter, H. H., Canzian, B., Henden, A. A., Levine, S. E., Luginbuhl, C. B., Monet, A. K. B., Monet, D. G., Pier, J. R., Stone, R. C., Walker, R. L., Burgasser, A. J., Gizis, J. E., Kirkpatrick, J. D., Liebert, J., & Reid, I. N. 2002, *AJ*, 124, 1170
- Dahn, C. C., Harris, H. C., Levine, S. E., Tilleman, T., Monet, A. K. B., Stone, R. C., Guetter, H. H., Canzian, B., Pier, J. R., Hartkopf, W. I., Liebert, J., & Cushing, M. 2008, *ApJ*, 686, 548
- Dupuy, T. J., Liu, M. C., & Ireland, M. J. 2009, *ApJ*, 692, 729
- Faherty, J. K., Burgasser, A. J., Cruz, K. L., Shara, M. M., Walter, F. M., & Gelino, C. R. 2009, *AJ*, 137, 1
- Gelino, C. R., Kulkarni, S. R., & Stephens, D. C. 2006, *PASP*, 118, 611
- Jameson, R. F., Casewell, S. L., Bannister, N. P., Lodieu, N., Keresztes, K., Dobbie, P. D., & Hodgkin, S. T. 2008, *MNRAS*, 384, 1399
- Joergens, V. 2008, *A&A*, 492, 545
- Joergens, V., & Müller, A. 2007, *ApJ*, 666, L113
- Kirkpatrick, J. D. 2005, *ARA&A*, 43, 195
- Kirkpatrick, J. D., Henry, T. J., & McCarthy, Jr., D. W. 1991, *ApJS*, 77, 417
- Kirkpatrick, J. D., et al. 1999, *ApJ*, 519, 802
- Knapp, G. R., et al. 2004, *AJ*, 127, 3553
- Konopacky, Q. M., Ghez, A. M., Barman, T. S., Rice, E. L., Bailey, III, J. I., White, R. J., McLean, I. S., & Duchene, G. 2010, *ApJ*, 711, 1087

- Lane, B. F., Zapatero Osorio, M. R., Britton, M. C., Martín, E. L., & Kulkarni, S. R. 2001, *ApJ*, 560, 390
- Liebert, J., & Burgasser, A. J. 2007, *ApJ*, 655, 522
- Liu, M. C., Dupuy, T. J., & Ireland, M. J. 2008, *ApJ*, 689, 436
- Liu, M. C., & Leggett, S. K. 2005, *ApJ*, 634, 616
- Liu, M. C., Leggett, S. K., Golimowski, D. A., Chiu, K., Fan, X., Geballe, T. R., Schneider, D. P., & Brinkmann, J. 2006, *ApJ*, 647, 1393
- Lloyd, J. P., Martinache, F., Ireland, M. J., Monnier, J. D., Pravdo, S. H., Shaklan, S. B., & Tuthill, P. G. 2006, *ApJ*, 650, L131
- Lodieu, N., Dobbie, P. D., Deacon, N. R., Hodgkin, S. T., Hambly, N. C., & Jameson, R. F. 2007, *MNRAS*, 380, 712
- Looper, D. L., Gelino, C. R., Burgasser, A. J., & Kirkpatrick, J. D. 2008a, *ApJ*, 685, 1183
- Looper, D. L., Kirkpatrick, J. D., & Burgasser, A. J. 2007, *AJ*, 134, 1162
- Looper, D. L., et al. 2008b, *ApJ*, 686, 528
- Luhman, K. L., Joergens, V., Lada, C., Muzerolle, J., Pascucci, I., & White, R. 2007a, *Protostars and Planets V*, 443
- Luhman, K. L., et al. 2007b, *ApJ*, 654, 570
- Martín, E. L., Brandner, W., & Basri, G. 1999, *Science*, 283, 1718
- Maxted, P. F. L., & Jeffries, R. D. 2005, *MNRAS*, 362, L45
- McElwain, M. W., & Burgasser, A. J. 2006, *AJ*, 132, 2074
- McLean, I. S., McGovern, M. R., Burgasser, A. J., Kirkpatrick, J. D., Prato, L., & Kim, S. S. 2003, *ApJ*, 596, 561
- Mohanty, S., Jayawardhana, R., Huélamo, N., & Mamajek, E. 2007, *ApJ*, 657, 1064
- Monet, D. G., Levine, S. E., Canzian, B., Ables, H. D., Bird, A. R., Dahn, C. C., Guetter, H. H., Harris, H. C., Henden, A. A., Leggett, S. K., Levison, H. F., Luginbuhl, C. B., Martini, J., Monet, A. K. B., Munn, J. A., Pier, J. R., Rhodes, A. R., Rieke, B., Sell, S., Stone, R. C., Vrba, F. J., Walker, R. L., Westerhout, G., Brucato, R. J., Reid, I. N., Schoening, W., Hartley, M., Read, M. A., & Tritton, S. B. 2003, *AJ*, 125, 984

- Muench, A. A., Lada, C. J., Luhman, K. L., Muzerolle, J., & Young, E. 2007, *AJ*, 134, 411
- Nakajima, T., Tsuji, T., & Yanagisawa, K. 2004, *ApJ*, 607, 499
- Pinfield, D. J., Dobbie, P. D., Jameson, R. F., Steele, I. A., Jones, H. R. A., & Katsiyannis, A. C. 2003, *MNRAS*, 342, 1241
- Pravdo, S. H., Shaklan, S. B., Wiktorowicz, S. J., Kulkarni, S., Lloyd, J. P., Martinache, F., Tuthill, P. G., & Ireland, M. J. 2006, *ApJ*, 649, 389
- Rayner, J. T., Toomey, D. W., Onaka, P. M., Denault, A. J., Stahlberger, W. E., Vacca, W. D., Cushing, M. C., & Wang, S. 2003, *PASP*, 115, 362
- Reid, I. N., Burgasser, A. J., Cruz, K. L., Kirkpatrick, J. D., & Gizis, J. E. 2001, *AJ*, 121, 1710
- Reid, I. N., Lewitus, E., Burgasser, A. J., & Cruz, K. L. 2006, *ApJ*, 639, 1114
- Schmidt, S. J., Cruz, K. L., Bongiorno, B. J., Liebert, J., & Reid, I. N. 2007, *AJ*, 133, 2258
- Sheppard, S. S., & Cushing, M. C. 2009, *AJ*, 137, 304
- Siegler, N., Close, L. M., Burgasser, A. J., Cruz, K. L., Marois, C., Macintosh, B., & Barman, T. 2007, *AJ*, 133, 2320
- Simons, D. A., & Tokunaga, A. 2002, *PASP*, 114, 169
- Stassun, K. G., Mathieu, R. D., & Valenti, J. A. 2006, *Nature*, 440, 311
- Stumpf, M. B., Brandner, W., Henning, T., Bouy, H., Koehler, R., Hormuth, F., Joergens, V., & Kasper, M. 2008, *ArXiv e-prints*
- Testi, L., D’Antona, F., Ghinassi, F., Licandro, J., Magazzù, A., Maiolino, R., Mannucci, F., Marconi, A., Nagar, N., Natta, A., & Oliva, E. 2001, *ApJ*, 552, L147
- Tokunaga, A. T., Simons, D. A., & Vacca, W. D. 2002, *PASP*, 114, 180
- Tuthill, P., Lloyd, J., Ireland, M., Martinache, F., Monnier, J., Woodruff, H., ten Brummelaar, T., Turner, N., & Townes, C. 2006, in Presented at the Society of Photo-Optical Instrumentation Engineers (SPIE) Conference, Vol. 6272, Society of Photo-Optical Instrumentation Engineers (SPIE) Conference Series
- Ushomirsky, G., Matzner, C. D., Brown, E. F., Bildsten, L., Hilliard, V. G., & Schroeder, P. C. 1998, *ApJ*, 497, 253

- Vacca, W. D., Cushing, M. C., & Rayner, J. T. 2003, *PASP*, 115, 389
- van Dam, M. A., et al. 2006, *PASP*, 118, 310
- West, A. A., Hawley, S. L., Bochanski, J. J., Covey, K. R., Reid, I. N., Dhital, S., Hilton, E. J., & Masuda, M. 2008, *AJ*, 135, 785
- Wilson, J. C., Miller, N. A., Gizis, J. E., Skrutskie, M. F., Houck, J. R., Kirkpatrick, J. D., Burgasser, A. J., & Monet, D. G. 2003, in *IAU Symposium*, Vol. 211, *Brown Dwarfs*, ed. E. Martín, 197
- Wizinowich, P. L., et al. 2006, *PASP*, 118, 297
- Zapatero Osorio, M. R., Lane, B. F., Pavlenko, Y., Martín, E. L., Britton, M., & Kulkarni, S. R. 2004, *ApJ*, 615, 958
- Zapatero Osorio, M. R., Martín, E. L., del Burgo, C., Deshpande, R., Rodler, F., & Montgomery, M. M. 2009, *A&A*, 505, L5